Short-channel functional near-infrared spectroscopy regressions improve when source-detector separation is reduced

James R. Goodwin
Chantel R. Gaudet
Andrew J. Berger

Short-channel functional near-infrared spectroscopy regressions improve when source-detector separation is reduced

James R. Goodwin,[a,b,*] **Chantel R. Gaudet,**[a] **and Andrew J. Berger**[a,c]
[a]University of Rochester, The Institute of Optics, Rochester, New York 14627, United States
[b]Queensland University of Technology, School of Chemistry, Physics and Mechanical Engineering, Brisbane, Queensland 4000, Australia
[c]University of Rochester, Department of Biomedical Engineering, Rochester, New York 14627, United States

Abstract. In functional near-infrared spectroscopy (fNIRS) of human cerebral hemodynamics, dedicated surface-sensitive recording channels are useful for regressing out background hemodynamics and isolating activation-specific responses. A wide variety of source-detector separations have been utilized for this purpose. Here, we report a direct comparison of regression performance between two extremes of the reported range, 13 and 6 mm. Measurements of visual stimulation response (flickering radial checkerboard) were obtained from nine adults using a standard commercial source-detector grid with 13-mm diagonals, into which three extra detector fibers were placed to provide 6-mm channels at certain locations. When the NIRS recordings (17 total trials) were processed, the contrast-to-noise ratio was significantly higher with 6-mm regression channels than with 13 mm. The advantage could be due in part to the undesired sensing of brain activity by the 13-mm channels. We suggest that shorter distances be considered for optimal removal of superficial hemodynamics in NIRS signals from the adult brain. © *The Authors. Published by SPIE under a Creative Commons Attribution 3.0 Unported License. Distribution or reproduction of this work in whole or in part requires full attribution of the original publication, including its DOI.* [DOI: 10.1117/1.NPh.1.1.015002]

1 Introduction

Near-infrared spectroscopic (NIRS) techniques provide the opportunity to monitor hemodynamic activity within the human head in a low-cost and noninvasive manner. Typically, light is sent into the head at the surface of the scalp and then detected at another location on the scalp, usually 20 to 40 mm away to ensure penetration through scalp and skull into the underlying cerebral tissue. Fluctuations in the detected signal are related to temporal changes in concentration of oxy- and deoxy-hemoglobin. Using the modified Beer-Lambert law (MBLL)[1,2] and two or more wavelengths in the NIR regime, concentration changes for both species of hemoglobin can be tracked and used as an indirect measure of neural activity.

Much NIRS work on cerebral hemodynamics is performed using continuous wave illumination and analyzed via single source-detector pairs. In such cases, signal averaging over multiple events is needed to isolate stimulus-related activations from uncorrelated hemodynamic trends (such as respiration and Mayer waves) that occur at similar amplitudes and temporal frequencies.[2,3] Recently, however, attempts have been made to measure the background hemodynamics explicitly and then subtract off some of its interference.[4–13] This is typically done using dedicated channels with reduced source-detector separations, such that the interrogation volume is confined primarily to extracerebral regions. In general, the short-distance measurement needs to be scaled or otherwise processed prior to any subtraction from the original source-detector time series measurement ("target channel"). Such processing can be performed using a variety of techniques that require no *a priori* knowledge of the specific optical properties of the human head. Fabbri et al.[14] first proposed using resting data to estimate the appropriate scaling factor for the two-measurement subtraction. Alternatively, the scaling factor can be calculated solely from the two time series themselves, using various strategies such as least-squares minimization,[7,9] adaptive filtering,[11–13] independent component analysis,[15] and state-space modeling with Kalman filtering.[4,5]

The literature exploring short-distance correction methods contains a range of separation distances between the source and the detector.[4–7,9–13] Saager et al.,[7] using least-squares subtraction, obtained improved contrast-to-noise ratios (CNRs) in a visual-stimulation study using a short-channel separation distance of 5 mm. In developing an adaptive-filter subtraction algorithm,[11] Zhang et al.[11–13] utilized a short-distance channel of 11 mm. Gregg et al.,[6] using a high-density array, regressed against an average of many 13-mm channels. Gagnon et al.[4,5] have explored multiple aspects of short-separation channel usage with a value of 10 mm.

This considerable range of short-distance values (from 5 to 15 mm) may reflect the fact that different extremes confer different benefits. The shortest separations are least sensitive to the cortex, providing a closer approximation to a "scalp only" signal for subtraction purposes. On the other hand, larger separations average over a larger scalp region, thus reducing the influence of

*Address all correspondence to: J. R. Goodwin, E-mail: james.goodwin@rochester.edu

spatial heterogeneity. To our knowledge, there has not been a dedicated experimental comparison of two different short-distance separations at the opposite ends of the current usage range.

A regression channel's proximity to the target channel (center-to-center separation) also affects how well the regression will reduce hemodynamic interference. Gagnon et al.[4] recently recommended that the regression channel's midpoint be within 15 to 20 mm of the target channel's to obtain substantial benefit. The report suggests that the decrease in performance at larger offsets is due to spatial inhomogeneity in the superficial hemodynamics.

This paper reports on a NIRS probe with dedicated pairs of regression channels with source-detector spacings of 13 mm ("short") and 6 mm ("very short"). This probe thus enables the same target channels to be corrected using either 6- or 13-mm data, with subsequent investigation of which method provides better detection of stimulus-related hemodynamic activations. The sections below describe the multiple-channel topographic instrument and probe design, a visual stimulation protocol, and the comparison of different regression approaches. Some observations about center-to-center channel distance and single-channel versus global-average regression are also provided.

2 Methods

2.1 Instrumentation

To enable comparisons between usage of "short" and "very short" regressors (henceforth, S and VS, respectively), we modified an existing commercial high-density fiber probe (Cephalogics LLC, Boston, Massachusetts; for details see Ref. 10). As shown in Fig. 1, the basic geometry of 24 sources and 21 detectors was an interleaved rectangular grid with overall dimensions of 13.2×6.6 cm. Nearest-neighbor diagonal distances were 13 mm, while the three next-nearest source-detector separations in the grid were 30, 39, and 47 mm.[6,10] The probe geometry was modified by moving three detectors (represented by dashed squares) to within 6 mm of sources in the grid. Three VS regression channels were thus created. For each, a single 13-mm channel sharing the same source was chosen as
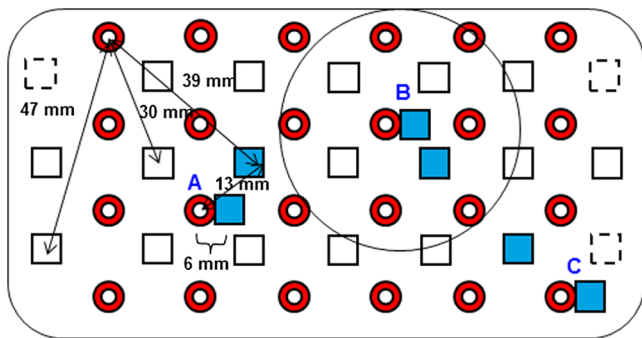

Fig. 1 Fiber bundle geometry for light delivery (circles) and detection (squares). In the unmodified regions of the rectangular grid, nearest-neighbor source-detector spacings are 13 mm (S channels), but relocated detectors are placed 6 mm from sources at labeled locations *A*, *B*, and *C* to provide three VS channels. The circle around location *B* (radius 25 mm) indicates the zone of target channels considered "near to *B*" in the data analysis; see text for details. N.B.: view from back (convex side) of the near-infrared spectroscopy headpiece. Key: dashed squares—vacated detector gridpoints, shaded squares—selected detectors for S/VS comparison.

an S channel for comparison in the subsequent data analysis. Figure 1 indicates the locations of these pairs of channels, labeled as *A*, *B*, and *C*.

At each of the 24 source positions, optical fiber bundles delivered NIR light-emitting diode light at two wavelengths (750 and 850 nm). The bundles were coupled to the head with a flexible, thermoplastic cap molded to fit the back of the head over the visual cortex. Each detector sampled light from all sources for a total of 672 possible measurements; of these, the 265 channels with source-detector separations of 47 mm or less were retained for analysis. Further details about the system's electronics have been published previously.[10]

Each time series of detected power at the two wavelengths was converted to changes in optical density and subsequently to changes in oxy- and deoxy-hemoglobin concentration times pathlength[16] using the modified Beer-Lambert law. To render the changes in familiar units of average micromolar over the optically explored volume, the values were divided by a differential pathlength factor (DPF) of 5. This particular DPF, close to values reported for adults by Duncan et al.,[17] does not affect any of the conclusions presented below and does not attempt to assign partial pathlength in the brain. Time series were high-pass filtered by subtracting a 25-s moving boxcar average and were low-pass filtered by performing a first-order Savitzky-Golay smooth[18] over a 4-s window.

2.2 Protocol

Visual stimulation was provided by a flickering black-and-white radial checkerboard pattern. The pattern was presented covering a 15-in. laptop screen, approximately 18 to 24 in. from the seated subject. During stimulus periods, the contrast of the pattern would reverse at a rate of 10 Hz. During rest periods, the subject was shown a solid gray screen with a small cross-hair in the center to maintain a central fixation point. The duration of the stimulations was 10 s, while the rest period was varied between 15 and 35 s to reduce habituation. A typical trial contained six visual stimulation epochs and lasted approximately 3 min.

Nine healthy subjects (age range: 19 to 40; four female) participated in this study, which was approved by the University of Rochester Research Subjects Review Board. Because most subjects sat for two trials, the total number of data runs was 17. The probe was placed over the occipital lobe, using the inion as a fiducial marker on the scalp. The center of the probe was placed approximately 1 to 2 cm above the inion, aligned along the midline. The probe's width of 13.2 cm was enough to span the right and left occipital cortex.

3 Analysis Methods

3.1 Correction Modalities

Every target channel's time series of oxyhemoglobin concentration change was processed six separate times, once using each of the correction channels (3 VS and 3 S). The regression process, which has been described previously,[8] performs scaled subtraction of the VS or S channel by least-squares minimization, producing a corrected time series. Each of the six regressions yielded a separate result. As a baseline for comparison, the data were also analyzed using no regressor at all.

Gagnon et al.[4] have reported that correction channels provide more benefit if they are located within approximately 20 mm of

the target channel, center-to-center. Since the headpiece in this study provided a range of center-to-center separations up to 40 mm, a wide range in correction quality was expected. For this reason, regressions were analyzed only for cases where the target channel's midpoint was within 25 mm of the VS regressor's midpoint (this radial distance from position B is indicated by the large circle in Fig. 1). Since the VS and S midpoints were not identical, the center-to-center separations from each target channel were also different. In regions A and B, there was no overall bias; in region C, the VS midpoint was always several millimeters farther away due to its placement at the edge of the probe. This created a bias against VS by reducing the spatial overlap, but since there were fewer channels corrected by C, the influence of this bias in the overall statistics was minor.

All target channels in our probe were within 25 mm of at least one 6 mm correction location (A, B, or C); some were that close to two.

3.2 Metrics

Noise-reduction methods are most relevant in cases where there is an underlying signal to detect. This study focused upon channels in which stimulus-evoked activation signals were observed. To compare the noise-reduction methods quantitatively, a performance metric had to be developed. We quantified performance based upon the CNR of the activation responses, as will be described shortly.

By sensing extracerebral hemodynamics, short-distance correction methods reduce their contribution in target-channel measurements, ideally leaving "brain-only" responses behind. When stimulus-evoked hemodynamic activity has occurred in the brain (i.e., in the case of a "true positive"), the correction process should increase the CNR of the NIRS measurement. Our chosen performance metric therefore implies that higher CNR correlates with better correction.

It must be noted, however, that stimulus-evoked activity can instead occur in the extracerebral vasculature, for example, via a flushing response. Since the evoked hemodynamic signature appears in the short-distance measurement as well, the correction process will tend to reduce it in the target channel recording. In such instances (the correction of a "false positive"), the hallmark of proper correction is now a decrease in CNR. In a study with roughly equal numbers of true and false positives, CNR would be a poor metric for successful signal correction. In order to use CNR as a metric in this study, it was necessary to create a situation where true positives greatly outweighed false positives. The validity and limitations of this assumption will be revisited after the results are reported.

3.2.1 Activation-flagged channels

Activation-flagged channels (AFCs) were defined in part by a net rise in oxyhemoglobin concentration during the stimulation interval, as in previous work.[9] Specifically, the average rise in oxy-hemoglobin concentration over the multiple stimulation epochs had to be significantly positive (one-sided t-test). The rise was calculated using 4-s windows centered on the onset and termination of the visual stimulus. For the t-test, the p-value was adjusted to account for multiple comparisons[19,20] by dividing the target threshold for significance by a value related to the number of independent recording channels N_I. In this case, the number of channels analyzed was 265, but the time series were not fully independent, due both to overlaps of

measurement volumes and to spatial correlations of hemodynamics over the measurement field. We chose a conservative, empirical value of $N_I = 100$ and a confidence level of 95%. With those inputs, the threshold for flagging activations was set at $p \leq 0.0005$ to determine whether the average rise in ΔHbO_2 was significantly greater than zero in any single channel. If a channel passed the t-test in any regression mode [VS, S, or no-regression (NR)], it passed to the second round of analysis.

3.2.2 CNR calculation

For each channel that passed the t-test, the corrected and uncorrected NIRS-measured oxyhemoglobin responses were each modeled using a skewed-Gaussian hemodynamic response function, as described previously.[9] A fit was performed for each stimulus epoch over a 25-s window, starting at the onset of the 10-s stimulus and ending 15 s after the conclusion of the stimulus. As shown in Fig. 2, "contrast" (C) is defined as the maximum amplitude of the skewed-Gaussian fit, and "noise" is defined as four times the standard deviation of the residual, thus giving barely visible signals a CNR of approximately unity. The average CNR of a channel's epochs served as an additional criterion for flagging activations ($\langle CNR \rangle > 1$). Specifically, this guarded against multipeaked hemodynamic oscillations that happen to pass the t-test by being randomly higher at the end of most epochs, but do not resemble single-peaked responses. In practice, all channels passing the t-test in these experiments also met the CNR criterion.

AFC status was assigned to a channel if the t-test and CNR criteria were both satisfied for at least one regression modality (S, VS, or NR).

3.2.3 Comparison of short-distance regression modalities using CNR values

As just noted, all correction modalities (including no-correction) participated equally in the selection of AFCs. This was done to eliminate bias.

The analysis consisted of testing whether one correction method (A) tended to produce higher or lower CNR values
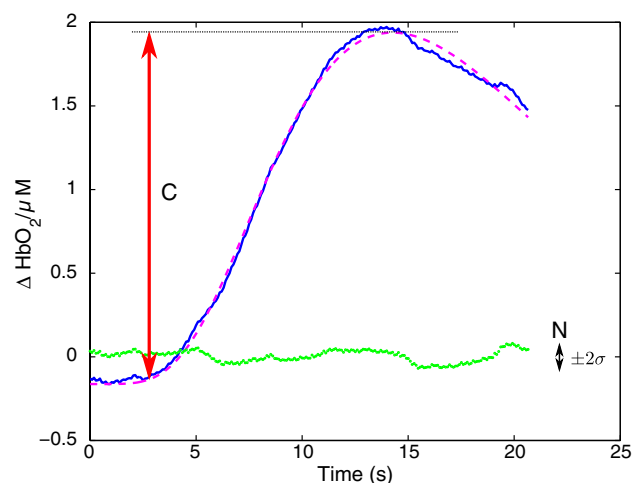

Fig. 2 An example of calculating contrast and noise values for a single stimulus epoch. The solid blue trace indicates the ΔHbO_2 time series after regression against a 6-mm (VS) channel. The skewed-Gaussian fit (dashed magenta) results in a noise residual (green) whose standard deviation is calculated.

than another method (B). Specifically, an additional two-sided t-test checked whether the average value of $\log[\mathrm{CNR}_A/\mathrm{CNR}_B]$ was significantly different from zero. A positive (negative) value meant that method $A(B)$ produced significantly larger CNR.

3.2.4 Global regression

Although the main purpose of this work was to compare different single correction channels at different separations, regression does not have to be performed using a single recording channel. Another option is to use an average over multiple channels that span a larger area of the head. This is a particularly attractive approach with high-density optode arrays intended for tomography (such as the probe for this study), where shallow-probing short-distance channels are already present. In this case, the multiple-channel average spatially characterizes the "shallow signal" over the entire area of study. Useful results of such "global average" regressions have been reported.[6]

The present headpiece had only three 6-mm channels, so a "global 6 mm" recording was not available. Thirteen-millimeter channels were present throughout the probe, however, and so the global average of the 13-mm channels was therefore calculated and used as yet another type of regressor for correction.

4 Results

Representative time-series data from one subject corresponding to one target channel (30-mm source-detector separation) are shown in Fig. 3. The uppermost trace (a) shows the oxyhemoglobin changes calculated using the target channel's detector alone. The fluctuations are not strongly associated with the visual-stimulation intervals (shown in gray). A very short (VS) 6-mm trace (b) was acquired nearby (in this case, sharing the same source location); it exhibits some of the same fluctuation features, as did the similar-looking S trace (c). When the VS trace (b) is least-squares subtracted from the original signal, the corrected response (trace d) exhibits a much stronger correlation with the stimulus onsets. (Epoch 9 of this corrected
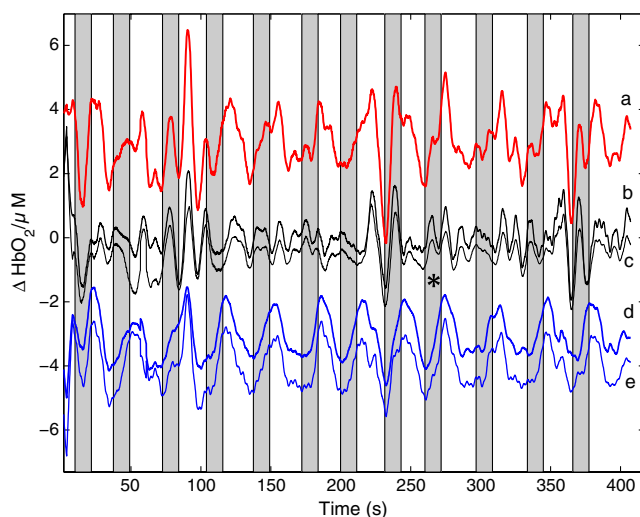
response, marked by an asterisk, was used to illustrate the CNR calculation in Fig. 2.) The associated correction using the S channel appears as trace (e).

Activation channels were flagged in 13 of the 17 total trials analyzed; these AFCs came from six of the nine subjects. In all, a total of 467 AFCs were designated. Different ways of analyzing the AFCs are discussed below.

4.1 VS versus NR

Figure 4 compares very-short regression to NR. Specifically, $\mathrm{CNR}_{6\ \mathrm{mm}}$ was calculated for each AFC and scatter-plotted against the corresponding value of $\mathrm{CNR}_{\mathrm{NR}}$. As noted above, a few target channels were within 25 mm of two VS channels (A, B, or C); these channels have two data points in this figure, corresponding to correction by two different 6-mm channels. The scatter plot clearly shows most points (317 out of 467) lying above a 45-deg line, suggesting that the regression improved the CNR on average. The two-sided t-test of $\log(\mathrm{CNR}_{6\ \mathrm{mm}}/\mathrm{CNR}_{\mathrm{NR}})$ confirmed that the improvement was significant ($p < 0.0001$). Significant improvement was also found for the S correction (data not shown). These results, consistent with prior work,[9] serve as a baseline check before proceeding to comparisons of different correction methods.

This scatter plot also reveals information about the relative prevalence of true and false positives among the AFCs. Of the data points where the CNR in one modality is at least 2× greater than the other, the larger CNR almost always belongs to the VS correction (i.e., such points lie above, not below, the unity line). According to the idealized model discussed earlier, if a correction method increases the CNR, this implies a true positive. Since almost all of the strong changes went in this direction, this suggests that the experimental design (adult volunteers watching a strong visual stimulus for many epochs) led to many more true positives than false positives.
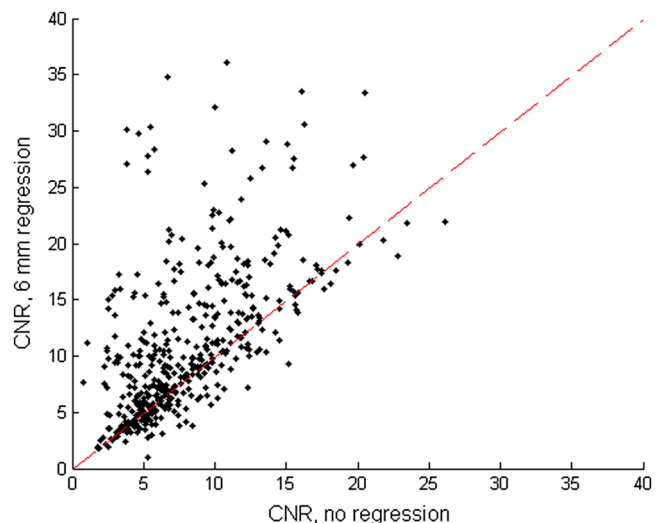

Fig. 3 Representative time courses of target, regressor, and "corrected" channels. (a) Large-separation target channel; (b, c) VS (6 mm) and S (13 mm) regressors; and (d, e) "corrected" responses using VS and S regressors.

Fig. 4 Scatter plot of contrast-to-noise ratio (CNR) from VS regression (6 mm) versus CNR from no-regression, for all "near-corrected" activation-flagged channels (AFCs) (correction channel 25 mm or closer to target channel, center-to-center). A dashed unity line is provided to guide the eye. 317 of the 467 data points have a higher CNR using VS regression, and the overall improvement is statistically significant ($p < 0.0001$; see text for details).

4.2 VS Versus S Regression

In Fig. 5, a scatter plot (similar to Fig. 4) compares $CNR_{6\ mm}$ to $CNR_{13\ mm}$, again for the cohort of all corrections within 25 mm. In this case, the number of data points above the 45-deg unity line is 326 out of 461. The smaller total number of data points, 461 compared to the 467 in Fig. 4, is due to six instances in which one of the S channels was itself flagged for activation; in these cases, S regression yielded an uninformative zero residual. The improvement was again statistically significant ($p < 0.0001$).

4.3 Global Regression

Since the global analysis could only be performed at 13 mm, there was no ability to compare global correction using VS and S modalities. Figure 6, however, illustrates an important relationship between the time course of a particular target channel (30 mm separation) and the global S average for that data run. As in Fig. 3, gray bars represent the stimulation epochs. The original 30-mm time series shows some amount of response correlated with the stimuli, but there is a lot of hemodynamic noise as well. In the corrected trace, plotted at the bottom, the hemodynamic interference is markedly reduced and the stimulus-related dynamics are noticeably smoother. No similar correction was observed in this case when a single nearby channel (either VS or S) was used as the regressor; the residual still contained most of the higher-frequency noise (data not shown).

In the example shown, the average CNR of the activations in the global regression was six times greater than the local regression (36 versus 6). Although this was an extreme example shown here for emphasis, the effect was not isolated. Averaging over all of the AFCs in this study, global-average S regression produced higher CNR values for 271 of the flagged channels, versus 196 being better with single-channel VS regression.
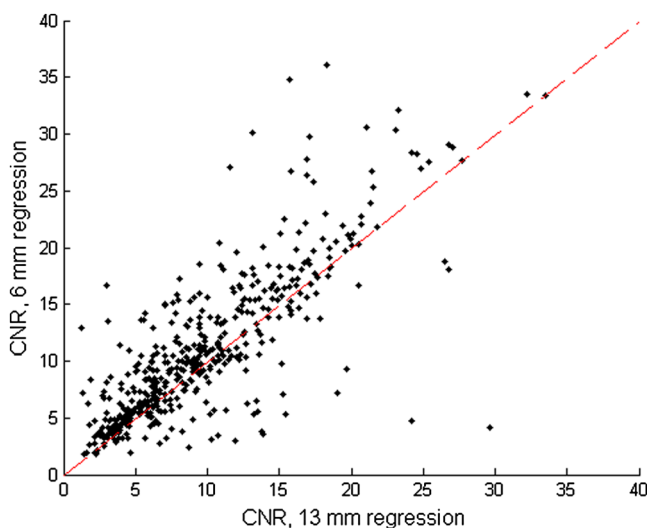
5 Discussion

5.1 VS Versus S Regression

As mentioned in Sec. 1, the major goal of this investigation was to compare two relevant source-detector separations for short-distance regressor channels. For this reason, the optical headpiece for this study was built with three pairs of regression channels at 6 and 13 mm, each pair sharing a common source. Time series from many target channels were then corrected using either 6-mm (VS) or 13-mm (S) channel data. Since the three relevant time series were acquired in parallel (target channel, VS regressor, and S regressor), all other variables were held fixed in the comparison of the regression results.

As Fig. 5 shows, overall the 6-mm VS regressor performed significantly better than the 13 mm S regressor, as measured by the CNR of the stimulus-related activations that were flagged. This suggests that 6 and 13 mm, although both regarded as distances too short to obtain an optimal sampling of the adult human cortex, are not functionally equivalent in terms of their hemodynamic probing.

One hypothesis for the difference in performance is that the 13-mm channel sensed some cortical hemodynamics itself. Using such a channel for regression would naturally subtract some of the signal one wishes to preserve. We have seen direct evidence of 13-mm channels containing significant activation signals in some of our data. For example, the upper trace in Fig. 7 shows a 13-mm NIRS time course collected from one of the subjects. No obvious stimulus-related features are apparent. When this channel is regressed against its associated 6-mm channel, however, the residual exhibits upward surges in oxyhemoglobin concentration at the onset of each stimulus block. In this instance, the 13-mm channel evidently contained significantly higher levels of cerebral activation signal than the 6-mm channel did. This would agree with the results in Fig. 5, where the CNR was statistically worse using 13-mm regression.
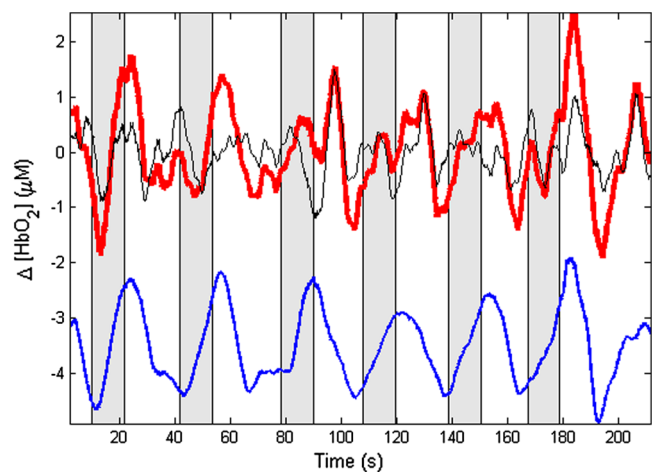

Fig. 5 Scatter plots of CNR from VS regression (6 mm) versus CNR from S regression (13 mm), for all "near-corrected" AFCs. In 326 out of 461 instances, the VS regression has higher CNR, and the overall improvement in CNR is statistically significant ($p < 0.0001$; see text for details).

Fig. 6 Oxyhemoglobin trends recorded using a single 30-mm channel (thick red upper trace) and the global average of the 13-mm channels (thin black upper trace, scaled for least-squares fit). Gray bars indicate stimulation epochs. The corrected time series (blue bottom trace) exhibits surges at the onset of each stimulation, with significant reduction in unrelated hemodynamic activity (e.g., around 95 s). In this instance, local correction provided no comparable reduction (data not shown).
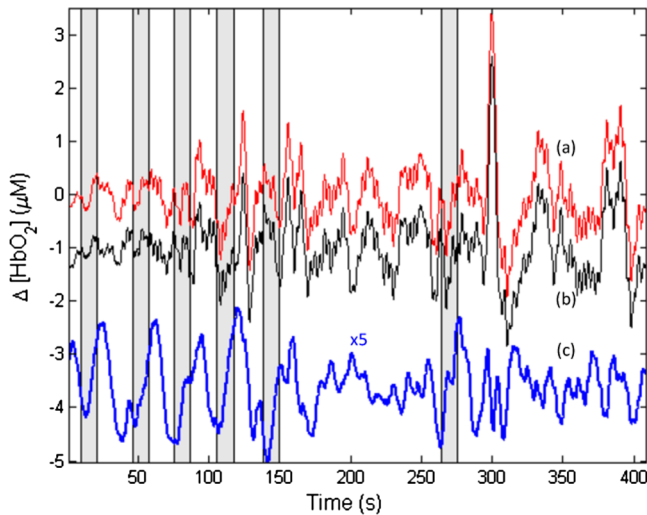
Fig. 7 Oxyhemoglobin trends recorded using a 13-mm channel (a, red) and the corresponding 6-mm channel sharing the same source (b, black, scaled for least-squares fit). Gray bars indicate stimulation epochs. The residual of the fit (c, blue, magnified for clarity by a factor of 5) exhibits surges at the onset of each stimulation, suggesting that the 13-mm recording has significant sensitivity to stimulus-related hemodynamics.

5.2 *Global Regression*

The global average at 13 mm sometimes provided a strong correction to a far-distance channel (cf. Fig. 6), and overall produced higher CNR than single-channel correction in a majority of cases. These findings emphasize that there are multiple potential sources of hemodynamic interference, and that no one correction approach is always the best choice. In the case where superficial hemodynamics are the dominant interferent, a local superficial channel ought to be the best regressor. In the case shown in Fig. 6, however, the dominant interference was better explained by a global average over a larger area. The "global interferent" in this case could have been predominantly in the brain, and thus poorly sampled by the VS channels.

This study leaves open the question of whether global regression is improved by switching to 6-mm channels, as was seen for single-channel regression. Such a comparison would require a probe with a full complement of 6-mm regression channels, which was not available in this study.

6 Conclusion

In NIRS measurements of stimulus-evoked hemodynamics, surface-sensitive recordings using short source-detector separations can help to eliminate nonspecific hemodynamic trends. In order to obtain the best CNR upon subtraction, we recommend based upon our statistical comparison that the source-detector separation be closer to 6 mm than 13 mm in measurements over the adult occipital cortex. The poorer performance seen at 13 mm could be at least partly due to undesired optical sampling of the activated brain region itself. These observations may extend to other regions of the adult head, and at smaller scales to infant measurements.

References

1. S. Wray et al., "Characterization of the near infrared absorption spectra of cytochrome aa3 and haemoglobin for the non-invasive monitoring of cerebral oxygenation," *Biochim. Biophys. Acta* **933**, 184–192 (1988).
2. F. Scholkmann et al., "A review on continuous wave functional near-infrared spectroscopy and imaging instrumentation and methodology," *NeuroImage* **85**, 6–27 (2014).
3. E. Kirilina et al., "The physiological origin of task-evoked systemic artefacts in functional near infrared spectroscopy," *NeuroImage* **61**, 70–81 (2012).
4. L. Gagnon et al., "Short separation channel location impacts the performance of short channel regression in NIRS," *NeuroImage* **59**, 2518–2528 (2012).
5. L. Gagnon et al., "Improved recovery of the hemodynamic response in diffuse optical imaging using short optode separations and state-space modeling," *NeuroImage* **56**, 1362–1371 (2011).
6. N. M. Gregg et al., "Brain specificity of diffuse optical imaging: improvements from superficial signal regression and tomography," *Front. Neuroenerg.* **2**, 14 (2010).
7. R. B. Saager, "Corrected near-infrared spectroscopy, C-NIRS: an optical system for extracting hemodynamic signatures unique to the brain," Ph.D. Thesis, University of Rochester (2008).
8. R. B. Saager and A. J. Berger, "Direct characterization and removal of interfering absorption trends in two-layer turbid media," *J. Opt. Soc. Am.* **22**, 1874–1882 (2005).
9. R. B. Saager, N. L. Telleri, and A. J. Berger, "Two-detector corrected near infrared spectroscopy (C-NIRS) detects hemodynamic activation responses more robustly than single-detector NIRS," *NeuroImage* **55**, 1679–1685 (2011).
10. B. W. Zeff et al., "Retinotopic mapping of adult human visual cortex with high-density diffuse optical tomography," *Proc. Natl. Acad. Sci. U. S. A.* **104**, 12169–12174 (2007).
11. Q. Zhang, E. N. Brown, and G. E. Strangman, "Adaptive filtering for global interference cancellation and real-time recovery of evoked brain activity: a Monte Carlo simulation study," *J. Biomed. Opt.* **12**, 044014 (2007).
12. Q. Zhang, E. N. Brown, and G. E. Strangman, "Adaptive filtering to reduce global interference in evoked brain activity detection: a human subject case study," *J. Biomed. Opt.* **12**, 064009 (2007).
13. Q. Zhang, G. E. Strangman, and G. Ganis, "Adaptive filtering to reduce global interference in non-invasive NIRS measures of brain activation: how well and when does it work?," *NeuroImage* **45**, 788–794 (2009).
14. F. Fabbri et al., "Optical measurements of absorption changes in two-layered diffusive media," *Phys. Med. Biol.* **49**, 1183–1201 (2004).
15. T. Funane et al., "Quantitative evaluation of deep and shallow tissue layers' contribution to fNIRS signal using multi-distance optodes and independent component analysis," *NeuroImage* **85**(Pt. 1), 150–165 (2014).
16. A. Maki et al., "Spatial and temporal analysis of human motor activity using noninvasive NIR topography," *Med. Phys.* **22**, 1997–2005 (1995).
17. A. Duncan et al., "Measurement of cranial optical path length as a function of age using phase resolved near infrared spectroscopy," *Pediatr. Res.* **39**, 889–894 (1996)..
18. A. Savitzky and M. J. E. Golay, "Smoothing and differentiation of data by simplified least squares procedures," *Anal. Chem.* **36**, 1627–1639 (1964).
19. D. Curran-Everett, "Multiple comparisons: philosophies and illustrations," *Am. J. Physiol. Regul. Integr. Comp. Physiol.* **279**(1), R1–R8 (2000).
20. A. Sassaroli et al., "Data analysis and statistical tests for near-infrared functional studies of the brain," *Proc. SPIE* **6850**, 685008 (2008).

Biographies of all authors are not available.